Thermoelectric Oxide Ceramics and Devices

Subjects: Materials Science, Ceramics

Contributor: Ping Zhang

Thermoelectric materials have gained wide attention to realize multilevel efficient energy management to alleviate the increasingly severe energy crisis. Oxide ceramics were well-explored as potential thermoelectric candidates because of their outstanding merits, including abundance, eco-friendliness, high-temperature stability, and chemical stability. A comprehensive summary of the diversified state-of-the-art oxide ceramics and establish the links between composition designing, preparation process, structural characteristics, and properties to summarize the underlying chemistry and physics mechanism of band engineering, doping, composited with the second phase, defects engineering, and entropy engineering is provided. Furthermore, advanced device design and applications such as thermoelectric modules, miniature generators, sensors, and coolers were summarized. Ultimately, the challenges and future perspective of oxides ceramics for the device design and thermoelectric applications in the development of energy harvesting technology have been prospected.

Keywords: thermoelectrics ; oxides ceramics ; ZT ; electrical conductivity ; phonon scattering

1. Introduction

Thermoelectric materials (TEs) have been used as a potential energy harvesting technology because they can convert heat into electricity and have no requirements for waste heat temperature [1][2][3]. Thermoelectric devices generally consist of *n*-type and *p*-type TEs wired electrically in series (or partly parallel) and thermally in parallel. Furthermore, there are also thermoelectric devices with single n-type and p-type TEs. They have the advantages of no moving parts, no noise, small size, etc., and have significant application merits in the military, aerospace, and high-tech energy fields [4][5].

It has been more than 200 years since the thermoelectric effect was discovered, and people have been constantly exploring and developing its industrial applications. In the early 1920s, Altenkirch, a German physicist, developed the fundamentals of thermoelectric power generation and refrigeration and summarized the performance evaluation parameters of TEs [6]: electrical conductivity (σ), Seebeck coefficient (S), and thermal conductivity (κ). Dimensionless thermoelectric merit ($ZT = S^2\sigma T/\kappa$, S is Seebeck coefficient, σ is electrical conductivity, T is absolute temperature, κ is thermal conductivity) is usually used as an indicator to measure the thermoelectric performance [7]. TEs with large ZT values must meet the requirements of a high Seebeck coefficient to ensure the generation of the obvious thermoelectric effect—high electrical conductivity leading to small Joule heat, large output power, as well as low thermal conductivity, are required to generate a substantial temperature difference. The above three thermoelectric parameters have a strong coupled relationship because they are dependent on the carrier concentration in a conflicting manner that restricts and influences each other, making how to optimize thermoelectric performance a huge challenge. Therefore, the coordinated regulation of S, σ, and κ to improve ZT has become the key point to realize the industrial application of thermoelectric materials.

2. Thermoelectric Fundamentals

Thermoelectric materials utilize the thermoelectric effect to achieve direct heat-to-electricity conversion. As shown in the schematic diagrams in **Figure 1**, the thermoelectric effect includes three effects: (i) the Seebeck effect, which transforms heat into electricity; (ii) the Peltier effect, absorption or release of heat at a junction in which there is an electric current; and (iii) the Thomson effect [1], the evolution or absorption of heat when an electric current passes through a circuit composed of a single material that has a temperature difference along its length. The most common application of the Seebeck effect is the widely existing thermocouple, which can be used in thermometers, thermoelectric power generation, and other thermal cycle fields. Static cooling is the major application of the Peltier effect. The Thomson effect establishes a connection between the previous two and reflects their differential influence.

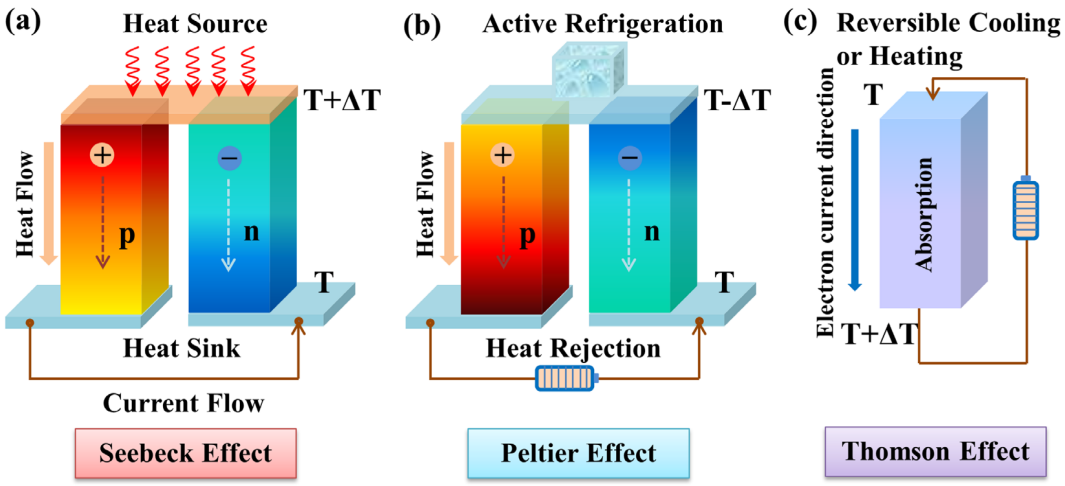

Figure 1. Schematic diagram of thermoelectric effects. (**a**) Seebeck effect for power generation, (**b**) Peltier effect for refrigeration, (**c**) Thomson effect for reversible cooling or heating.

3. Fabrication of Thermoelectric Oxide Ceramics

3.1. Lattice Structures of Thermoelectric Oxide Ceramics

3.1.1. n-Type Thermoelectric Oxides

As an *n*-type thermoelectric oxide, strontium titanate ($SrTiO_3$) has attracted widespread interest due to its high effective mass of carriers, chemical and thermal stability at high temperatures, and high structural tolerance. $SrTiO_3$ has a cubic perovskite structure and Pm3m space group at room temperature, and its lattice constant is a = b =c = 3.905 Å [8]. In a unit cell unit connected by solid lines in the figure, Ti^{4+} ions occupy the central position in the unit cell, Sr^{2+} ions occupy the eight vertex positions, O^{2-} ions form an oxygen octahedron at the center of six faces of the cubic unit cell, and Ti^{4+} ions occupied the octahedral gaps. Therefore, the coordination number of Sr^{2+} ions is 12, and the coordination number of Ti^{4+} ions is 6. From another perspective, there is a cubic unit cell structure composed of eight Ti-O octahedrons in strontium titanate. Eight Ti-O octahedrons are located at the eight top corners of the cubic structure, while Sr^{2+} ions occupy the center of the cubic structure. The direct band gap of $SrTiO_3$ is 3.2 eV, and its σ is very low. Its phase transitions from cubic to tetragonal will occur at temperatures below 105 K [9].

3.1.2. p-Type Thermoelectric Oxides

$Ca_3Co_4O_9$ is a typical representative material in *p*-type thermoelectric oxides. A rock salt type Ca_2CoO_3 layer sublattice and CdI 2 type CoO_2 slabs alternated arrangement into the layered structure of $Ca_3Co_4O_9$ [10][11]. Along the c-axis, it can be seen as a sandwich construction (rock salt plate sandwiched between two plates). $Ca_3Co_4O_9$ belongs to the monoclinic system structure, which is a C2/m superspace group. The incommensurate structure consists of two layers with distinct lattice parameters, a = 4.8323 Å, b1 = 2.82 Å, b2 = 4.55 Å, c = 10.8428 Å, β = 98.13°, allocated to 2.82 Å cells of CoO_2 subsystem (b1) and 4.55 Å cells of Ca_2CoO_3 subsystem (b2).

BiCuSeO is a *p*-type oxide TE with excellent thermoelectric properties. It has a tetragonal crystal structure (a = b =3.9273 Å, c = 8.9293 Å, Z = 2) with symmetry of P4/nmm (No. 129) space group [12]. BiCuSeO possesses a layered “hybrid” crystal structure in which the conductive layer $(Cu_2Se_2)^{2-}$ alternates with the insulating layer $(Bi_2O_2)^{2+}$ [13][14]. The bond length of Bi-Se is 3.2 Å, which is larger than that of Bi-O of 2.33 Å, indicating that it has layer characteristics [12]. The $(Cu_2Se_2)^{2-}$ sublayer is the main conductive channel, called the conductive layer, which can be used to regulate electrical properties; the $(Bi_2O_2)^{2+}$ sublayer is a non-conductive layer (insulating layer), which can be effectively used for thermal conductivity suppression. Therefore, the layered structure of BiCuSeO-based compounds can achieve collaborative optimization of thermal and electrical conductivities (**Figure 2**).

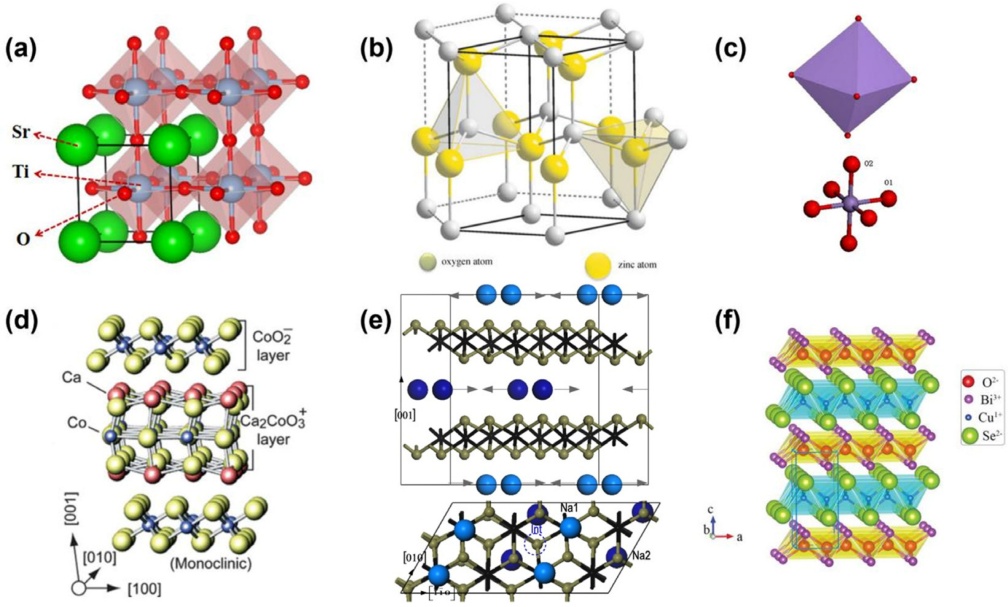

Figure 2. Schematic of the crystal structure of thermoelectric oxides. (**a**) $SrTiO_3$, (**b**) ZnO [15], (**c**) $CaMnO_3$ [16], (**d**) $Ca_3Co_4O_9$ [17], (**e**) Na_xCoO_2 [18], (**f**) BiCuSeO [19].

3.2. Preparation Method

3.2.1. Bulk Crystal Growth

It is reported that for *p*-type layered oxide TEs, the thermoelectric properties of single crystals are much higher than those of polycrystalline samples for a given component. For example, the figure merit *ZT* of single crystal Na_xCoO_2 and $Ca_3Co_4O_9$ samples reach 1.2 and 0.87, respectively, and the performance of polycrystalline samples is generally only about half of that of single crystal samples. Fujita et al. used the flux technique to prepare $Na_xCoO_{2-\delta}$ single crystals and measured their high-temperature thermoelectric properties for the first time. At 800 K, the *PF* reaches 7.7 $mWm^{-1}K^{-2}$, and the *ZT* value reaches 1.2 [20].

3.2.2. Solid-State Method

The solid-state reaction method is the most widely employed method for preparing different oxide TEs [21][22][23][24][25][26]. Generally, two solid-state steps are required for the synthesis of polycrystalline oxide TEs, which mainly includes the preparation of pre-sintered powder, and then sintered compact bulk ceramic samples suitable for testing various properties. The high-purity solid precursor powders were mixed and calcined at high temperatures, such as TiO_2 and $SrCO_3$, required for the synthesis of strontium titanate [27]. This approach possesses the advantage of simplicity and low cost, but generally, the synthetic product after a high-temperature calcination process is blocky and requires a secondary ball milling to obtain fine powders to maintain high reactivity to sinter ceramics.

Adopting sintering aids is a commonly used method to improve the bulk density of ceramics in the traditional solid-state sintering process. The sintering aids have the following functions: (1) Forming a liquid phase environment and increasing the diffusion driving force of particles; (2) increasing ceramic density and controlling grain size; (3) preventing the polycrystalline transformation of the matrix material; and (4) entering into the lattice of the matrix material to form solid solutions during the later stage of sintering. At present, the common sintering aids include Bi_2O_3, CuO, V_2O_5, and B_2O_3, etc. [28][29][30][31][32].

3.2.3. Spark Plasma Sintering

Spark plasma sintering (SPS) technology is also commonly utilized to prepare bulk oxide TEs [33][34][35][36][37][38]. SPS is also known as Pulse Electric Current Sintering (PECS). During the sintering process, the discharge plasma generated at the moment when the electrode is connected to the DC pulse current makes each particle inside the powder produce Joule heat uniformly and activate the particle surface, which makes it easy to prepare uniform, dense, and high-quality ceramic samples.

3.2.4. Mechanical Alloying

Mechanical alloying is a method to obtain solid alloy or solid solution by high-speed ball milling or grinding. Mechanical alloying has gained widespread attention for its advantages of a short cycle, low energy consumption, and simple process. Liu et al. studied the synthesis of La-doped $SrTiO_3$ nanopowders using mechanical alloying in an air atmosphere.

In comparison to the solid-phase reaction method, the mechanical alloying technique can eliminate the calcination stage and is more cost-effective and eco-friendly [39].

3.2.5. Liquid-Phase Synthesis

Colloidal Synthesis

Solid-phase reaction method has the disadvantages of low purity and high energy consumption. To overcome the shortcoming of the high-temperature solid-phase method, the hydrothermal synthesis and sol-gel method became aroused researchers' attention.

The materials synthesized by the sol-gel method generally use inorganic salt or organic alkoxide as the precursor and, through a chemical reaction such as hydrolysis polymerization, nucleation, and growth transform from liquid precursors to sol and then to a network structure known as a 'gel', and then after dried and heating treatment to obtain the target material.

Hydrothermal Synthesis

The hydrothermal method is a solution reaction-based approach and can synthesize nanomaterials, which have been successfully applied for the preparation of TEs [40]. Usually, hydrothermal synthesis may occur over a wide temperature range from ambient temperature to extremely high temperatures and requires high-pressure conditions to generate high vapor pressures to trigger the chemical reaction or to control the morphology.

Solvothermal Synthesis

The solvothermal synthesis is analogous to the hydrothermal method and is based on heating the precursors and a solvent in a closed system at a temperature above the boiling point of the solvent used [27]. The synthetic procedure usually requires high temperature and high pressure to create the supercritical circumstances to develop the peculiar behavior of the solvent, exerting different influences on the precursors resulting in the desired product. Park et al. synthesized Ag-$SrTiO_3$ nanocomposites by one-pot solvothermal method [41] using strontium nitrate ($Sr(NO_3)_2$), silver (I) nitrate ($AgNO_3$), and titanium tetraisopropoxide $[(CH_3)_2CHO]_4Ti$ (TTIP) as starting ingredients. Furthermore, the loading quantity of Ag could be easily manipulated by adjusting the concentration of the $AgNO_3$ precursor. In addition, the thermoelectric properties of layered TEs can be effectively controlled by bottom-up wet chemical synthesis of two-dimensional nanosheets/nanoplates [42][43][44].

4. Development and Strategies to Improve the Thermoelectric Performance of Oxide Ceramics

Several of the selection rules are somewhat paradoxical as a result of the inherent trade-off effect between σ and S. Many optimized strategies may have a complicated correlated impact on S, σ, and κ. As an illustration, the increase of doping concentration will improve σ while decreasing S. Then, Ioffe's finding in doped semiconductors was the first effort to empirically determine the carrier concentration "sweet spot" of excellent thermoelectrics is $n = 10^{18}$–10^{20} cm^{-3} [45]. Consequently, an optimal power factor ($PF = S^2\sigma$) versus doping concentration exists at a relatively high doping level. Furthermore, a further decrease of κ is necessary to produce a high ZT.

4.1. Band Engineering

Since S, σ, and κ of TEs are determined by the transport and interaction of carriers and phonons, adjusting one parameter often may sacrifice other physical parameters, making achieving collaborative optimization of thermoelectric performance a huge challenge. In bulk TEs, the band gap, the degeneracy of the conduction band, the extreme value of the valence band, and the effective mass in the band structure are fundamental parameters that determine the thermoelectric performance. According to the Mott formula [46], the parameter of S is in direct proportion to the slope of the energy band near the Fermi level. A greater slope means a greater S. Furthermore, the S is a function of the variation of σ near the Fermi surface, and increasing the complexity of the crystal structure can increase the complexity and the degeneracy of the band structure, leading to more extreme values in the conduction band and valence band, thus increasing S. In a word, factors of the band gap, energy band shape, effective mass of carriers, mobility, etc., determined by band structure are closely related and produce a trade-off effect on thermoelectric performa

4.2. Doping

Element doping is one of the widely used basic strategies to regulate carrier concentration for enhancing the thermoelectric performance of TEs. By properly doping elements with different valence states into different cationic lattice sites, a well-regulated *n* can be obtained, which leads to an optimized $S^2\sigma$. Doping will cause a change in cell parameters, induce point defects, and bring lattice distortion because of the position of atoms and the length of valence bonds changed, resulting in variations of *S,* κ, and σ. Furthermore, the length and strength of the valence bond is an important parameter that determines thermal conductivity.

In *n*-type $SrTiO_3$-based TEs, trivalent states of La [32][34][39][40][46][47][48][49], Ce [49], Nd [49], Sm [49][50], Gd [49], Dy [49], Pr [51], and Y [52] can be used to dope in Sr^{2+} site. The valence states of $\geq 5^+$, such as Ta [53], Nb [54], and W [55], can be used to dope in the Ti^{4+} site. K. Singsoog et al. [56] investigated the influence of La doping amount on $Sr_{1-x}La_xTiO_3$ (x = 0, 0.06, 0.13, 0.25) through theoretical calculation; the results show that the parameters (*S*, σ, κ, *PF*, and *ZT*) increase first and then decrease. When the doping concentration of La = 0.13, it has the best thermoelectric performance of S_{900K} = −450 μ V/*K*, PF_{1200K} = 2.55 mW/m/K^2.

In the *n*-type $CaMnO_3$ system, three types of elements doped at the Ca position are rare earth elements (La, Y, Ce, Sm, Pu, Nd, Lu, etc.) [57][58], main group elements such as Bi [59] and alkaline earth elements (Ba, Sr, Mg, etc.) [60]. Additionally, the doped elements in the Mn site mainly include Ta, V, Nb, Ru, etc. [61]. The doping cases such as $Ca_{1-x}Bi_xMnO_3$ ($0 \leq x \leq 0.10$) [59], $CaMn_{1-x}Nb_xO_3$ (x = 0.02, 0.05, 0.08) [62], Dy and Yb co-doping on $Ca_{1-2x}Dy_xYb_xMnO_3$ ($0 \leq x \leq 0.10$) [63], and $Ca_{0.92-x}Pr_{0.08}Sr_xMnO_3$ (x = 0.01, 0.02, 0.03, 0.04) [64] demonstrated that Bi, Nb, Dy, Yb, Pr doping at $CaMnO_3$ obtained the *ZT* values range of 0.18–0.27 which were much improved compared with the pure phase of $CaMnO_3$ (*ZT* = 0.04).

To improve the thermoelectric properties of ZnO, commonly used doping elements are C, Si, Fe, In, Ga, Al, Ni, and Sb [21][65][66][67]. Among them, Al-doped ZnO is the one widely studied and has the best TE performance at present. In the case of $Zn_{0.96}Al_{0.02}Ga_{0.02}O$ [65], *ZT* = 0.65 at 1247 K was obtained, which is one of the high levels of *ZT* values in n-type oxide thermoelectric materials. Additionally, this outstanding achievement can be attributed to the Al and Ga co-doping can significantly reduce the thermal conductivity from 40 W/m/K of $Zn_{0.98}Al_{0.02}O$ to 5 W/m/K of $Zn_{0.93}Al_{0.02}Ga_{0.05}O$.

In the p-type $Ca_3Co_4O_9$-based TEs, much research focused on the partial substitution of cations on the Ca-site such as Na [68], Sr [69], Ba [70], La [71], Ag [71], Fe [72], Pb [73], Ag [74], Ga [75], Tb [76], and Yb [77], while Ni [78], Mn [79], Cu [79], and Ir [80] were introduced into the Co-site to optimize the thermoelectric properties in the $Ca_3Co_4O_9$ system. Specifically, as R^{3+} has a higher ox

4.3. Entropy Engineering

Due to its superior characteristics, such as low thermal conductivity [26][28][81][82][83], high-entropy ceramics (HECs) containing five or more cations have lately gained considerable interest in the TE field. High-entropy engineering has been confirmed to increase the *S* and reduce the κ_l in TE oxide ceramics, making it a promising strategy for optimizing thermoelectric performance by broadening the composition design. High-throughput screening has been used to construct multi-component TEs with high entropy, as reported by Zhang et al. [84] and Liu et al. [85]. By decreasing the κ_l and/or increasing *S*, high-entropy engineering can become an efficient technique to considerably improve thermoelectric performance (**Figure 3**).

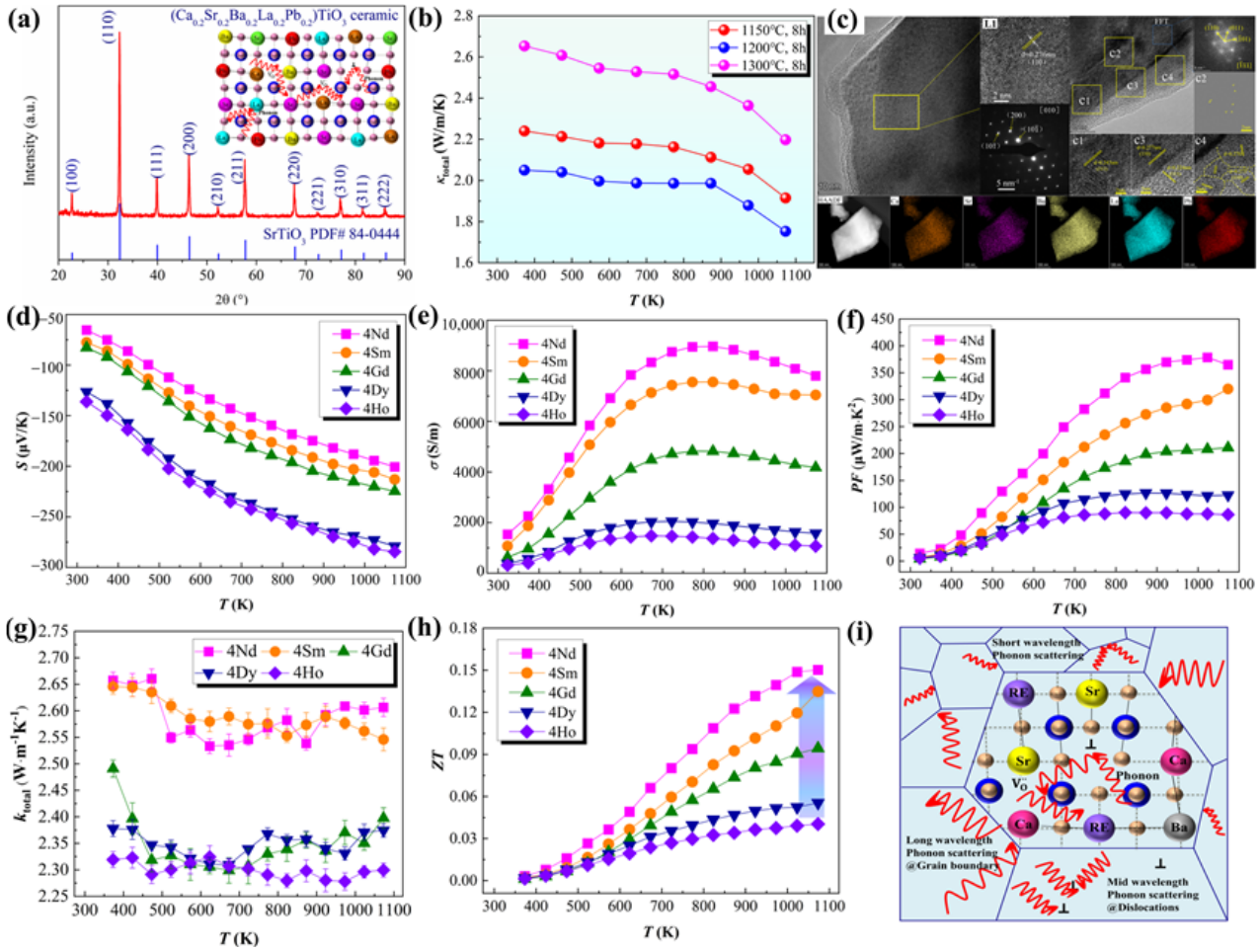

Figure 3. (**a**) XRD patterns, (**b**) κ, (**c**) TEM results of the high-entropy $(Ca_{0.2}Sr_{0.2}Ba_{0.2}La_{0.2}Pb_{0.2})TiO_3$ ceramics [86]. (**d**–**h**) S, σ, PF, κ_{total}, and ZT values of the high-entropy $(Sr_{0.2}Ca_{0.255}Ba_{0.25}RE_{0.25})TiO_3$ ceramics [87]. (**i**) Schematic diagram of the possible phonon scattering in reducing lattice thermal conductivity for high-entropy ceramic [88].

4.4. Defect Engineering

In ionic compounds, the heat transport mechanism is dominated by κ_l. Additionally, κ_l can be lowered due to phonon scattering. Based on Debye–Callaway's model and the relaxation-time approximation, the κ is a function of phonon scattering rates ($1/\tau$) or the relaxation time (τ) [89]. τ has contributions from grain boundary scattering (τ_B), point defect scattering (τ_{PD}), phonon-phonon Umklapp scattering (τ_U), and electron-phonon scattering (τ_{ep}) as represented by Equation (8) [89][90].

Here, v_m is the mean acoustic velocity, L is the average grain size, Θ_D is the Debye temperature, ω is the phonon frequency, and A, B, and C are parameters corresponding to the point defects, Umklapp process, and electron-phonon scattering, respectively. Phonons are more likely to be strongly scattered by lattice defects of considerable size. Therefore, during the defect regulation, attention should be paid to building a full-scale hierarchical structure containing defects of various forms and scales to achieve "total phonon scattering" in a broad frequency range. Specifically, the atomic scale point defects, such as vacancy, replacement atoms, etc., can realize effective phonon scattering by the high-frequency short wavelength [81][83] (**Figure 4** and **Figure 5**).

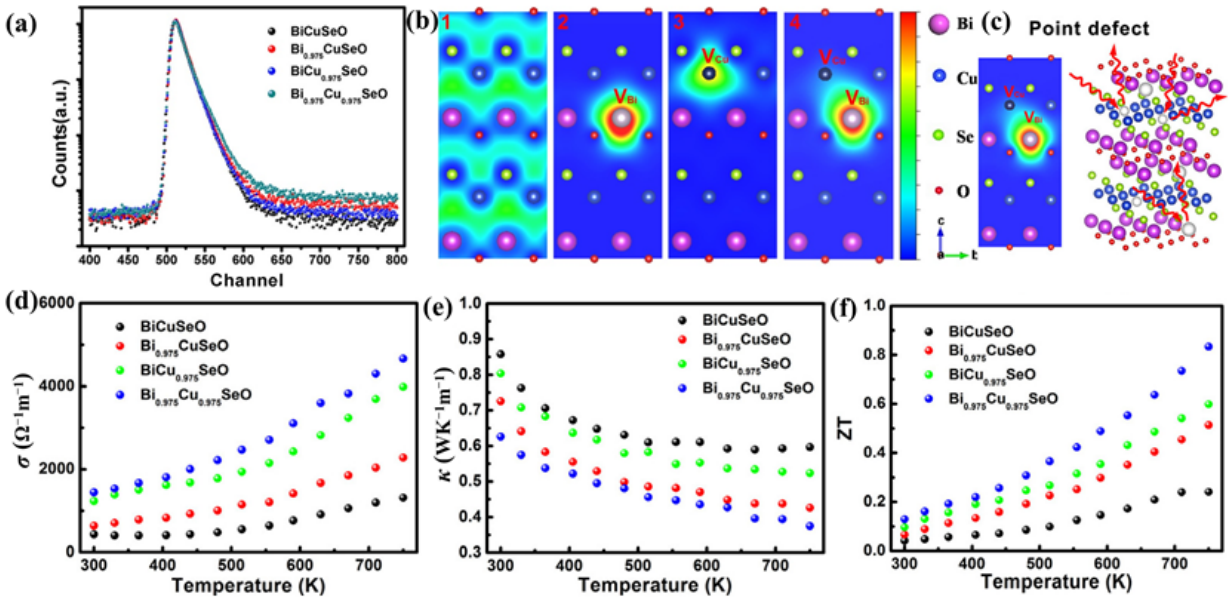

Figure 4. (**a**) Positron lifetime spectrum. (**b**) Schematic representation of trapped positrons for $Bi_{1-x}Cu_{1-y}SeO$ samples in (100) plane. (**c**) Schematic representation of phonon scattering with Bi/Cu vacancies. (**d**–**f**) σ, κ, and ZT values of the $Bi_{1-x}Cu_{1-y}SeO$ samples [91].

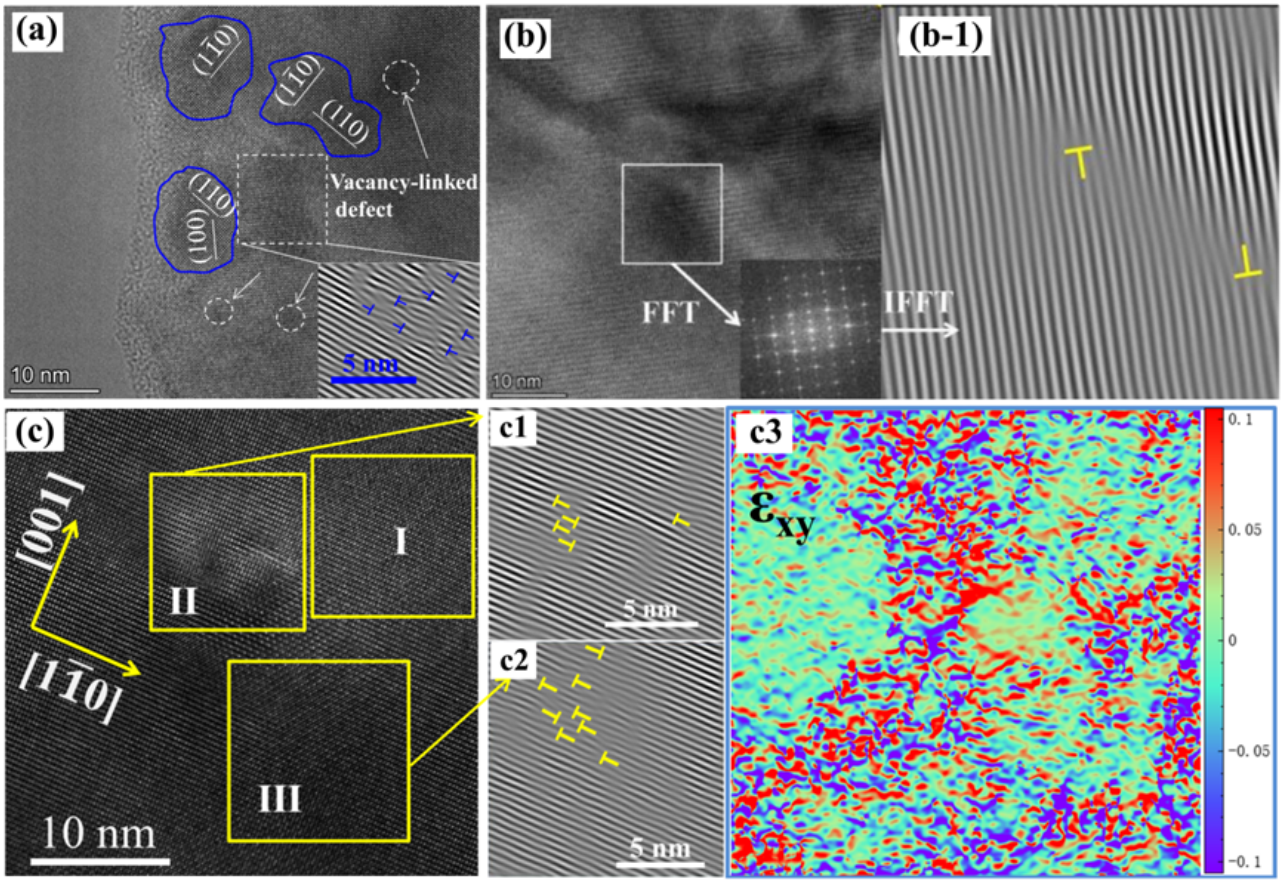

Figure 5. (**a**) HRTEM images of the $(Sr_{0.25}Ca_{0.25}Ba_{0.25}RE_{0.25})TiO_3$ sample [88], (**b**) HRTEM images and the corresponding FFT image and IFFT image (b-1) along the [92] zone axis of the $Sr_{0.9}La_{0.1}(Zr_{0.25}Sn_{0.25}Ti_{0.25}Hf_{0.25})O_3$ sample [93], (**c**) HRTEM images and the corresponding IFFT images (c1 and c2) and strain map (c3) by geometric phase analysis (GPA) method [94].

4.5. Grain Boundary and Nanostructure Engineering

Grain boundaries (GBs) form ubiquitous microstructures in polycrystalline oxide ceramics, which play a significant role in tuning their ZT. Different grain size has a varied impact on σ and κ. To ensure that the effect of GBs or/and the nanostructure on decreasing κ is larger than its deterioration in σ, the grain sizes should be appropriately tuned. The energy filtering mechanism was proposed, meaning that randomly distributed potential barriers can filter away low-energy carriers to cause a decrease in the actual carrier density to improve S. In the nanostructured polycrystalline ceramic TEs, low energy carrier filtering effects combined with the enhanced phonon scattering can effectively suppress κ_l [32][40][95][96][97], confirmed by both computational and experimental results.

Optimized thermoelectric performance by grain boundary and nanostructure are mainly reflected in lowering κ [40][98], or the formation of a conductive path at grain boundary to promote the carrier mobility; these two factors play a synergistic effect on the electron and phonon transport process contribute to a trade-off ZT values of 0.3–0.4. In the cases of the nanostructured $Sr_{0.91}La_{0.09}TiO_3$ sample, ZT = 0.37 was achieved at 973 K [99], a greatly improved performance ZT = 0.35 in Pr-doped of $SrTiO_{3-\delta}$ because of the Pr-rich grain boundaries contributed to improving carrier mobility [99][100], and the improving ZT = 0.38 obtained in $Sr_{0.8}La_{0.067}Ti_{0.8}Nb_{0.2}O_{3-\delta}$ system containing Cu or Fe inclusions [101].

4.6. Textured Engineering

Texture engineering offers a strategy for gaining better thermoelectric performance in bulk ceramics by creating crystallographic anisotropy. Especially in layered crystal structure TEs, the electron and phonon transport properties are highly anisotropic. Multi-scale parallel interfaces, including zigzag interfaces and “core-shell” interfaces inside the orientation of the stripe-like grains, the paralleled grain boundaries, and lattice stacking faults were observed in the “brick-wall” microstructure can contribute to suppressing the thermal conductivity [71][102]. The physical properties of this special crystallographic orientation in textured ceramics can approach 60–80% of the properties of single crystals of the same composition. Creating the textured structure helps to the decoupling of electrical and thermal properties (**Figure 6**).

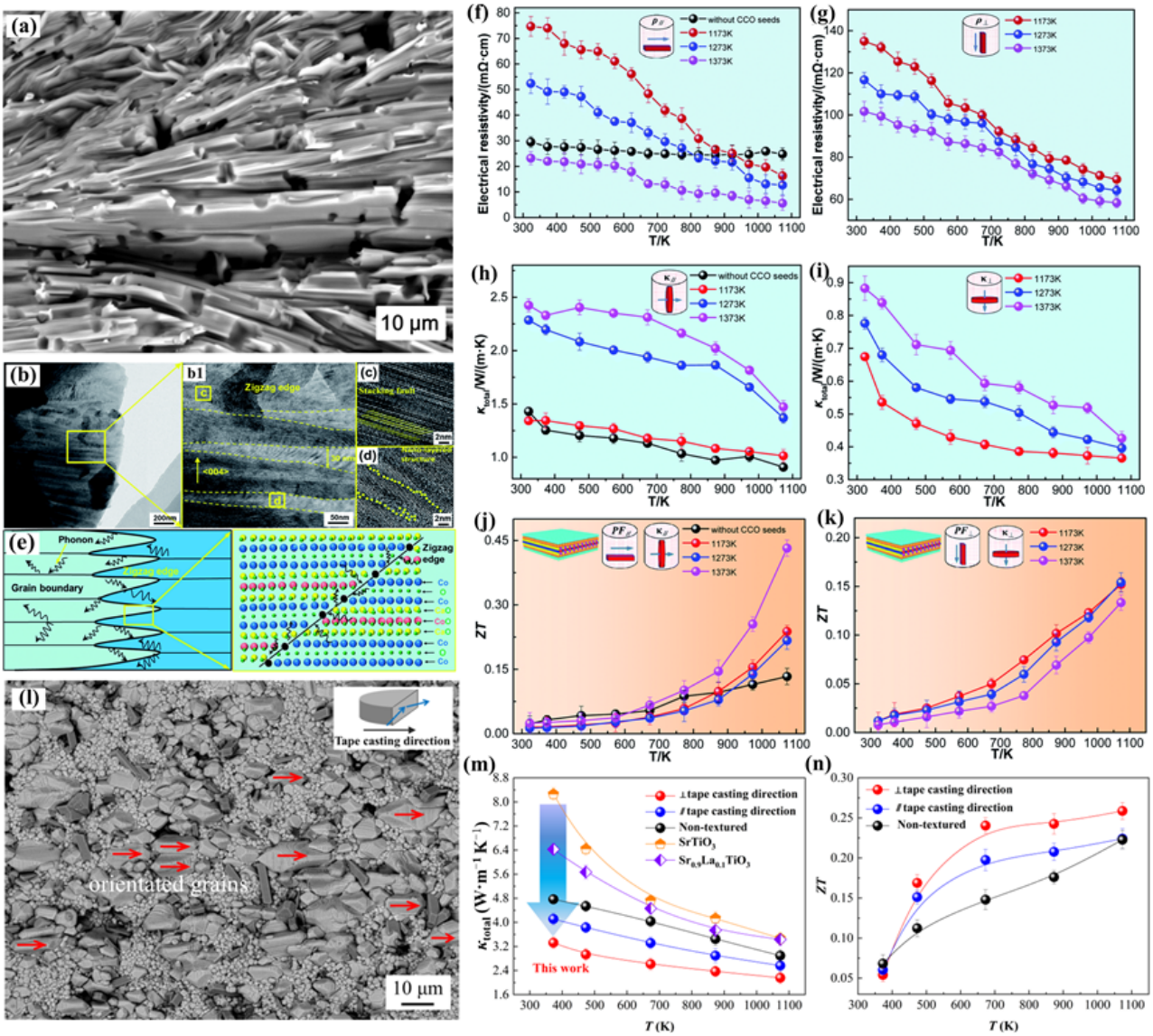

Figure 6. (**a**) BSE image, (**b**–**d**) TEM images, and (**e**) the sketch diagram of phonon scattering at the grain boundary and zigzag edge of the $(Ca_{0.87}Ag_{0.1}La_{0.03})_3Co_4O_9$ textured ceramics, and temperature dependence of the thermoelectric properties of the samples in parallel and perpendicular to the tape-casting direction. (**f**,**g**) Electrical resistivity, (**h**,**i**) thermal conductivity, (**j**,**k**) ZT values [103]. (**l**) BSE image, (**m**) Total thermal conductivity, and (**n**) ZT values of the $Sr_{0.9}La_{0.1}TiO_3$-based textured ceramic [104].

4.7. Composites

For the ionic compound of oxide ceramics, their resistivity after doping modification, nanostructuring, or entropy engineering is still relatively high. To further reduce the resistivity of oxide ceramics, some compounds with excellent

electrical conductivity, such as metal particles, graphene, and its derivatives, are added to the matrix to improve the thermoelectric properties.

In addition, it has been confirmed that the 2D graphene can be introduced into $SrTiO_3$-based ceramics for grain refinement and promoting more oxygen vacancy formation to enhance carrier mobility [105]. Therefore, $SrTiO_3$-based ceramics containing graphite or its derivatives achieve single-crystal-like electron mobility [105][106][107][108] because the delocalization of Anderson localized electrons aided by graphite leads to a manifold improvement in weighted mobility and further the enhanced electron transport properties.

5. Device Applications

5.1. Power Generation

In recent years, thermoelectric modules have attracted wide attention due to their great potential for power generation and electronic refrigeration. At present, oxide thermoelectric devices can be used in a wide temperature range, especially in high temperatures, but there are few types of research focused on oxide thermoelectric devices, and the efficiency and power of thermoelectric conversion still need to be further improved. Most of these modules are made of $Ca_3Co_4O_9$ as *p*-type materials, and the most common thermoelectric *n*-type oxides are $CaMnO_3$, $SrTiO_3$, ZnO, etc. [109]. TE modules usually adopt the silver bar and silver paste [110], Cu, Ni, etc., as electrode contacts.

5.2. Sensor Devices

One of the primary applications of TEs is the temperature sensors, namely thermocouples, in which the temperature measurement of thin film thermocouples belongs to the contact in situ temperature measurement technology. For example, indium tin oxide (ITO) -In_2O_3 film thermocouple [111] have a limit measuring temperature reaching 1300 °C and the Seebeck coefficient reaches 160 μV/°C, the $MoSi_2$-Al_2O_3 and $TaSi_2$-Al_2O_3 thin film thermocouple [112] prepared by screen printing technology presented the thermoelectric output of 16 mV at the high-temperature stage.

5.3. Flexibility and Wearable Devices

Flexible thermoelectric materials with excellent plastic deformation, light, inconspicuous, and other characteristics have a widespread application in portable electronic devices and wearable devices. Due to the ductility of inorganic semiconductors and ceramic insulators rarely observed, the application of inorganic oxides in flexible TEs field is rarely reported.

5.4. Other Application

Other applications of thermoelectric modules include aerospace, automotive waste heat recovery systems, refrigeration, etc. At present, the application of alloy thermoelectric has been well-researched, while oxide needs to be further studied.

Recently, organic-inorganic composites and hybrid materials have promoted a flexible TE devices' design and exploration, which can be used in wearable electronic devices, and sensors to apply to the "Internet of Things" (IoT) field [113] with the spring-up and development of novel two-dimensional (2D) materials growth, superlattice growth, and inorganic-organic composites. Furthermore, using of high-performance nanostructured TEs combined with spectrally selective solar absorbers to develop solar thermoelectric generators (STEGs) obtained a peak efficiency of 4.6% [114], opening up the door to the comprehensive application of TEs for energy conversion.

References

1. Zebarjadi, M.; Esfarjani, K.; Dresselhaus, M.S.; Ren, Z.F.; Chen, G. Perspectives on thermoelectrics: From fundamentals to device applications. Energy Environ. Sci. 2012, 5, 5147–5162.
2. He, J.; Tritt, T.M. Advances in thermoelectric materials research: Looking back and moving forward. Science 2017, 357, eaak9997.
3. Zhu, K.; Deng, B.; Zhang, P.X.; Kim, H.S.; Jiang, P.; Liu, W.S. System efficiency and power: The bridge between the device and system of a thermoelectric power generator. Energy Environ. Sci. 2020, 13, 3514–3526.
4. Bu, Z.L.; Zhang, X.Y.; Hu, Y.X.; Chen, Z.W.; Lin, S.Q.; Li, W.; Xiao, C.; Pei, Y.Z. A record thermoelectric efficiency in tellurium-free modules for low-grade waste heat recovery. Nat. Commun. 2022, 13, 237.

5. Biswas, K.; He, J.Q.; Blum, I.D.; Wu, C.; Hogan, T.P.; Seidman, D.N.; Dravid, V.P.; Kanatzidis, M.G. High-performance bulk thermoelectrics with all-scale hierarchical architectures. Nature 2012, 489, 414–418.
6. Altenkirch, E. Elektrothermische Kälteerzeugung und reversible elektrische Heizung. Phys. Z. 1911, 12, 920–924.
7. Goupil, C.; Seifert, W.; Zabrocki, K.; Müller, E.; Snyder, G.J. Thermodynamics of thermoelectric phenomena and applications. Entropy 2011, 13, 1481–1517.
8. Mitchell, R.H.; Chakhmouradian, A.R.; Woodward, P.M. Crystal chemistry of perovskite-type compounds in the tausonite-loparite series, (Sr1−2xNaxLax)TiO3. Phys. Chem. Miner. 2000, 27, 583–589.
9. Nelmes, R.J.; Meyer, G.M.; Hutton, J. Thermal motion in SrTiO3 at room temperature: Anharmonic or disordered? Ferroelectrics 1978, 21, 461–462.
10. Yang, W.C.; Zhang, H.C.; Tao, P.G.; Zhang, D.D.; Zhang, D.W.; Wang, Z.H.; Tang, G.D. Optimization of the spin entropy by incorporating magnetic ion in a misfit-layered calcium cobaltite. Ceram. Int. 2016, 42, 9744–9748.
11. Wu, T.; Tyson, T.A.; Bai, J.M.; Pandya, K.; Jaye, C.; Fischer, D. On the origin of enhanced thermoelectricity in Fe doped Ca3Co4O9. J. Mater. Chem. C 2013, 1, 4114–4121.
12. Zhao, L.D.; He, J.Q.; Berardan, D.; Lin, Y.H.; Li, J.F.; Nan, C.W.; Drago, N. BiCuSeO oxyselenides: New promising thermoelectric materials. Energy Environ. Sci. 2014, 7, 2900–2924.
13. Liu, Y.; Zhao, L.D.; Zhu, Y.C.; Liu, Y.C.; Li, F.; Yu, M.J.; Liu, D.B.; Xu, W.; Lin, Y.H.; Nan, C.W. Synergistically optimizing electrical and thermal transport properties of BiCuSeO via a dual-doping approach. Adv. Energy Mater. 2016, 6, 1502423.
14. Yang, D.W.; Su, X.L.; Yan, Y.G.; Hu, T.Z.; Xie, H.Y.; He, J.; Uher, C.; Kanatzidis, M.G.; Tang, X.F. Manipulating the combustion wave during self-propagating synthesis for high thermoelectric performance of layered oxychalcogenide Bi1−xPbxCuSeO. Chem. Mater. 2016, 28, 4628–4640.
15. Schröer, P.; Krüger, P.; Pollmann, J. First-principles calculation of the electronic structure of the wurtzite semiconductors ZnO and ZnS. Phys. Rev. B 1993, 47, 6971–6980.
16. Zhang, F.P.; Lu, Q.M.; Zhang, X.; Zhang, J.X. First principle investigation of electronic structure of CaMnO3 thermoelectric compound oxide. J. Alloys Compd. 2011, 509, 542–545.
17. Ohta, H.; Sugiura, K.; Koumoto, K. Recent progress in oxide thermoelectric materials: P-type Ca3Co4O9 and n-type SrTiO3. Inorg. Chem. 2008, 47, 8429–8436.
18. Assadi, M.H.N.; Katayama-Yoshida, H. Restoration of long range order of Na ions in NaxCoO2 at high temperatures by sodium site doping. Comput. Mater. Sci. 2015, 109, 308–311.
19. Liu, Y.; Zhao, L.D.; Zhu, Y.C.; Liu, Y.C.; Li, F.; Yu, M.J.; Liu, D.B.; Xu, W.; Lin, Y.H.; Nan, C.W. Synergistically optimizing electrical and thermal transport properties of BiCuSeO via a dual-doping approach. Adv. Energy Mater. 2016, 6, 1502423.
20. Fujita, K.; Mochida, T.; Nakamura, K. High-temperature thermoelectric properties of NaxCoO2-delta single crystals. Jpn. J. Appl. Phys. 2001, 40, 4644–4647.
21. Zhu, B.B.; Chen, C.; Yao, Z.C.; Chen, J.Y.; Jia, C.; Wang, Z.H.; Tian, R.M.; Tao, L.; Xue, F.; Hng, H.H. Multiple doped ZnO with enhanced thermoelectric properties. J. Eur. Ceram. Soc. 2021, 41, 4182–4188.
22. Kovalevsky, A.V.; Aguirre, M.H.; Populoh, S.; Patricio, S.G.; Ferreira, N.M.; Mikhalev, S.M.; Fagg, D.P.; Weidenkaff, A.; Frade, J.R. Designing strontium titanate-based thermoelectrics: Insight into defect chemistry mechanisms. J. Mater. Chem. A 2017, 5, 3909–3922.
23. Hassanin, H.; Jiang, K. Net shape manufacturing of ceramic micro parts with tailored graded layers. J. Micromech. Microeng. 2014, 24, 015018.
24. Hassanina, H.; Jiang, K. Fabrication and characterization of stabilised zirconia micro parts via slip casting and soft moulding. Scr. Mater. 2013, 69, 433–436.
25. Wang, T.; Nan, P.F.; Wang, H.C.; Wang, H.; Su, W.; Sotelo, A.; Zhai, J.Z.; Wang, X.; Ran, Y.Z.; Chen, T.T.; et al. Right heterogeneous microstructure for achieving excellent thermoelectric performance in Ca0.9R0.1MnO3−δ(R.=Dy, Yb) Ceramics. Inorg. Chem. 2018, 57, 9133–9141.
26. Zhang, P.; Lou, Z.H.; Qin, M.H.; Xu, J.; Zhu, J.T.; Shi, Z.M.; Chen, Q.; Reece, M.J.; Yan, H.X.; Gao, F. High-entropy (Ca0.2Sr0.2Ba0.2La0.2Pb0.2)TiO3 perovskite ceramics with A-site short-range disorder for thermoelectric applications. J. Mater. Sci. Technol. 2022, 97, 182–189.
27. Kovalevsky, A.V.; Yaremchenko, A.A.; Populoh, S.; Populoh, S.; Frade, J.R. Enhancement of thermoelectric performance in strontium titanate by praseodymium substitution. J. Appl. Phys. 2013, 113, 053704.

28. Lou, Z.H.; Zhang, P.; Gong, L.Y.; Xu, J.; Gong, L.Y.; Reece, M.J.; Yan, H.X.; Gao, F. A novel high-entropy perovskite ceramics Sr0.9La0.1(Zr0.25Sn0.25Ti0.25Hf0.25)O3 with low thermal conductivity and high Seebeck coefficient. J. Eur. Ceram. Soc. 2022, 42, 3480–3488.

29. Han, J.; Song, Y.; Liu, X.; Wang, F.P. Sintering behavior and thermoelectric properties of LaCoO3 ceramics with Bi2O3-B2O3-SiO2 as a sintering aid. RSC Adv. 2014, 4, 51995–52000.

30. Alvarez-Ruiz, D.T.; Azough, F.; Hernandez-Maldonado, D.; Kepaptsoglou, D.M.; Ramasse, Q.M.; Day, S.J.; Svec, P.; Svec, P.; Freer, R. Utilising unit-cell twinning operators to reduce lattice thermal conductivity in modular structures: Structure and thermoelectric properties of Ga2O3(ZnO)9. J. Alloys Compd. 2018, 762, 892–900.

31. Nishiyama, S.; Ichikawa, A.; Hattori, T. Thermoelectric properties of CuO-added AgSbO3 ceramics. J. Ceram. Soc. Jpn. 2004, 112, 298–300.

32. Azough, F.; Gholinia, A.; Alvarez-Ruiz, D.T.; Duran, E.; Kepaptsoglou, D.M.; Eggeman, A.S.; Ramasse, Q.M.; Freer, R. Self-nanostructuring in SrTiO3: A novel strategy for enhancement of thermoelectric response in oxides. ACS Appl. Mater. Interfaces 2019, 11, 32833–32843.

33. Shi, Z.M.; Wang, L.X.; Li, L.L.; Wei, J.; Tong, S.J.; Zhang, J.Z.; Li, X.T.; Guo, Y.P.; Zhang, Y. Joint effect of Bi2O3 and CuO additives in regulating the thermoelectric properties of (Ca0.87Ag0.1Dy0.03)3Co4O9 composite ceramics. Mater. Sci. Eng. B 2023, 290, 116311.

34. Wang, Y.F.; Zhang, X.Y.; Shen, L.M.; Bao, N.Z.; Wan, C.L.; Park, N.H.; Koumoto, K.; Gupta, A. Nb-doped grain boundary induced thermoelectric power factor enhancement in La-doped SrTiO3 nanoceramics. J. Power Sources 2013, 241, 255–258.

35. Tian, T.; Cheng, L.H.; Xing, J.J.; Zheng, L.Y.; Man, Z.Y.; Hu, D.L.; Bernik, S.; Zeng, J.T.; Yang, J.; Liu, Y. Effects of sintering on the microstructure and electrical properties of ZnO-based thermoelectric materials. Mater. Des. 2017, 132, 479–485.

36. Diaz-Chao, P.; Giovannelli, F.; Lebedev, O.; Chateigner, D.; Lutterotti, L.; Delorme, F.; Guilmeau, E. Textured Al-doped ZnO ceramics with isotropic grains. J. Eur. Ceram. Soc. 2014, 34, 4247–4256.

37. Qin, M.J.; Lou, Z.J.; Shi, Z.J.; Zhang, R.J.; Xu, J.; Gao, F. Enhanced thermoelectric properties of Sr0.9La0.1TiO3 ceramics fabricated by SPS with nanosized Ti addition. J. Mater. Sci.-Mater. Electron. 2020, 31, 6919–6926.

38. Chen, Y.X.; Shi, K.D.; Li, F.; Xu, X.; Ge, Z.H.; He, J.Q. Highly enhanced thermoelectric performance in BiCuSeO ceramics realized by Pb doping and introducing Cu deficiencies. J. Am. Ceram. Soc. 2019, 102, 5989–5996.

39. Liu, D.Q.; Zhang, Y.W.; Kang, H.J.; Li, J.L.; Chen, Z.N.; Wang, T.M. Direct preparation of La-doped SrTiO3 thermoelectric materials by mechanical alloying with carbon burial sintering. J. Eur. Ceram. Soc. 2018, 38, 807–811.

40. Park, K.; Son, J.S.; Woo, S.I.; Shin, K.; Oh, M.W.; Park, S.D.; Hyeon, T. Colloidal synthesis and thermoelectric properties of La-doped SrTiO3 nanoparticles. J. Mater. Chem. A 2014, 2, 4217–4224.

41. Park, D.; Ju, H.; Kim, J. One-pot fabrication of Ag-SrTiO3 nanocomposite and its enhanced thermoelectric properties. Ceram. Int. 2019, 45, 16969–16975.

42. Mehta, R.J.; Zhang, Y.L.; Karthik, C.; Singh, B.; Siegel, R.W.; Borca-Tasciuc, T.; Ramanath, G. A new class of doped nanobulk high-figure-of-merit thermoelectrics by scalable bottom-up assembly. Nat. Mater. 2012, 11, 233–240.

43. Populoh, S.; Trottmann, M.; Aguire, M.H.; Weidenkaff, A. Nanostructured Nb-substituted CaMnO3 n-type thermoelectric material prepared in a continuous process by ultrasonic spray combustion. J. Mater. Res. 2011, 26, 1947–1952.

44. Sun, Y.F.; Cheng, H.; Gao, S.; Liu, Q.H.; Sun, Z.H.; Xiao, C.; Wu, C.Z.; Wei, S.P.; Xie, Y. Atomically thick bismuth selenide freestanding single layers achieving enhanced thermoelectric energy harvesting. J. Am. Chem. Soc. 2012, 134, 20294–20297.

45. Dehkordi, A.M.; Zebarjadi, M.; He, J.; Tritt, T.M. Thermoelectric power factor: Enhancement mechanisms and strategies for higher performance thermoelectric materials. Mater. Sci. Eng. R 2015, 97, 1–22.

46. Wang, J.; Zhang, B.Y.; Kang, H.J.; Li, Y.; Yaer, X.B.; Li, J.F.; Tan, Q.; Zhang, S.; Fan, G.H.; Liu, C.Y.; et al. Record high thermoelectric performance in bulk SrTiO3 via nano-scale modulation doping. Nano Energy 2017, 35, 387–395.

47. Qin, M.J.; Lou, Z.H.; Zhang, P.; Shi, Z.M.; Xu, J.; Chen, Y.S.; Gao, F. Enhancement of thermoelectric performance of Sr0.9La0.1TiO3-based ceramics regulated by nanostructures. ACS Appl. Mater. Interfaces 2020, 48, 53899–53909.

48. Qin, M.J.; Gao, F.; Dong, G.G.; Xu, J.; Fu, M.S.; Wang, Y.; Reece, M.; Yan, H.X. Microstructure characterization and thermoelectric properties of Sr0.9La0.1TiO3 ceramics with nano-sized Ag as additive. J. Alloys Compd. 2018, 762, 80–89.

49. Kovalevsky, A.V.; Yaremchenko, A.A.; Populoh, S.; Thiel, P.; Fagg, D.P.; Weidenkaff, A.; Frade, J.R. Towards a high thermoelectric performance in rare-earth substituted SrTiO3: Effects provided by strongly-reducing sintering conditions.

Phys. Chem. Chem. Phys. 2014, 16, 26946–26954.

50. Putri, Y.E.; Said, S.M.; Refinel, R.; Ohtaki, M.; Syukri, S. Low thermal conductivity of RE-doped SrO(SrTiO3)1 Ruddlesden Popper phase bulk materials prepared by molten salt method. Electron. Mater. Lett. 2018, 14, 556–562.
51. Kahalya, M.U.; Schwingenschlögl, U. Thermoelectric performance enhancement of SrTiO3 by Pr doping. J. Mater. Chem. A 2014, 2, 10379–10383.
52. Ito, M.; Ohira, N. Effects of TiB2 addition on spark plasma sintering and thermoelectric performance of Y-doped SrTiO3 synthesized by polymerized complex process. Compos. Part B Eng. 2016, 88, 108–113.
53. Cui, Y.; Salvador, J.R.; Yang, J.; Wang, H.; Amow, G.; Kleinke, H. Thermoelectric properties of heavily doped n-type SrTiO3 bulk materials. J. Electron. Mater. 2009, 38, 1002–1007.
54. Zhang, B.Y.; Wang, J.; Zou, T.; Zhang, S.; Yaer, X.B.; Ding, N.; Liu, C.Y.; Miao, L.; Li, Y.; Wu, Y. High thermoelectric performance of Nb-doped SrTiO3 bulk materials with different doping levels. J. Mater. Chem. C. 2015, 3, 11406–11411.
55. Kovalevsky, A.V.; Populoh, S.; Patrício, S.G.; Thiel, P.; Ferro, M.C.; Fagg, D.P.; Frade, J.R.; Weidenkaff, A. Design of SrTiO3-based thermoelectrics by tungsten substitution. J. Phys. Chem. C 2015, 119, 4466–4478.
56. Singsoog, K.; Seetawan, T.; Vora-Ud, A.; Thanachayanont, C. Theoretical enhancement of thermoelectric properties of Sr1−xLaxTiO3. Integr. Ferroelectr. 2014, 155, 111–118.
57. Flahaut, D.; Mihara, T.; Funahashi, R.; Nabeshima, N.; Lee, K.; Ohta, H.; Koumoto, K. Thermoelectrical properties of A-site substituted Ca1−xRexMnO3 system. J. Appl. Phys. 2006, 100, 084911.
58. Sanmathi, C.S.; Takahashi, Y.; Sawaki, D.; Klein, Y.; Retoux, R.; Terasaki, I.; Noudem, J.G. Microstructure control on thermoelectric properties of Ca0.96Sm0.04MnO3 synthesised by co-precipitation technique. Mater. Res. Bull. 2010, 45, 558.
59. Kabir, R.; Tian, R.M.; Zhang, T.S.; Donelson, R.; Tan, T.T.; Li, S. Role of Bi doping in thermoelectric properties of CaMnO3. J. Alloys Compd. 2015, 628, 347–351.
60. Kuganathan, N.; Chroneos, A. Defect and dopant properties in CaMnO3. AIP Adv. 2021, 11, 055106.
61. Xu, G.J.; Funahashi, R.; Pu, Q.R.; Liu, B.; Tao, R.H.; Wang, G.S.; Ding, Z.J. High-temperature transport properties of Nb and Ta substituted CaMnO3 system. Solid State Ion. 2004, 171, 147–151.
62. Bocher, L.; Aguirre, M.H.; Logvinovich, D.; Shkabko, A.; Robert, R.; Trottmann, M.; Weidenkaff, A. CaMn1−xNbxO3 (x ≤ 0.08) perovskite-type phases as promising new high-temperature n-type thermoelectric materials. Inorg. Chem. 2008, 47, 8077–8085.
63. Zhu, Y.H.; Su, W.B.; Liu, J.; Zhou, Y.C.; Li, J.C.; Zhang, X.H.; Du, Y.L.; Wang, C.L. Effects of Dy and Yb co-doping on thermoelectric properties of CaMnO3 ceramics. Ceram. Int. 2015, 41, 1535–1539.
64. Liu, K.K.; Liu, Z.Y.; Zhang, F.P.; Zhang, J.X.; Yang, X.Y.; Zhang, J.W.; Shi, J.L.; Ren, G.; He, T.W.; Duan, J.J. Improved thermoelectric performance in Pr and Sr Co-doped CaMnO3 materials. J. Alloys Compd. 2019, 808, 151476.
65. Ohtaki, M.; Araki, K.; Yamamoto, K. High thermoelectric performance of dually doped ZnO ceramics. J. Electron. Mater. 2009, 38, 1234–1238.
66. Pham, A.T.T.; Luu, T.A.; Pham, N.K.; Thi, H.K.; Nguyen, T.H.; Hoang, D.V.; Lai, H.T.; Tran, V.C.; Park, J.H.; Lee, J.K.; et al. Multi-scale defects in ZnO thermoelectric ceramic materials co-doped with In and Ga. Ceram. Int. 2020, 46, 10748–10758.
67. Zhang, D.B.; Zhang, B.P.; Ye, D.S.; Liu, Y.C.; Li, S. Enhanced Al/Ni co-doping and power factor in textured ZnO thermoelectric ceramics prepared by hydrothermal synthesis and spark plasma sintering. J. Alloys Compd. 2016, 656, 784–792.
68. Constantinescu, G.; Rasekh, S.; Torres, M.A.; Bosque, P.; Diez, J.C.; Madre, M.A.; Sotelo, A. Effect of Na doping on the Ca3Co4O9 thermoelectric performance. Ceram. Int. 2015, 41, 10897–10903.
69. Zhang, L.; Liu, Y.; Tan, T.T.; Liu, Y.; Zheng, J.; Yang, Y.L.; Hou, X.J.; Feng, L.; Suo, G.Q.; Ye, X.H.; et al. Thermoelectric performance enhancement by manipulation of Sr/Ti doping in two sublayers of Ca3Co4O9. J. Adv. Ceram. 2020, 9, 769–781.
70. Constantinescu, G.; Rasekh, S.; Torres, M.A.; Madre, M.A.; Sotelo, A.; Diez, J.C. Improvement of thermoelectric properties in Ca3Co4O9 ceramics by Ba doping. J. Mater. Sci. Mater. Electron. 2015, 26, 3466–3473.
71. Shi, Z.M.; Su, T.C.; Zhang, P.; Lou, Z.H.; Qin, M.J.; Gao, T.; Xu, J.; Zhu, J.H.; Gao, F. Enhanced thermoelectric performance of Ca3Co4O9 ceramics through grain orientation and interface modulation. J. Mater. Chem. A 2020, 8, 19561–19572.

72. Delorme, F.; Diaz-Chao, P.; Giovannelli, F. Effect of Ca substitution by Fe on the thermoelectric properties of Ca3Co4O9 ceramics. J. Electroceram. 2018, 40, 107–114.

73. Demirel, S.; Altin, E.; Oz, E.; Altin, S.; Bayri, A. An enhancement ZT and spin state transition of Ca3Co4O9 with Pb doping. J. Alloys Compd. 2015, 627, 430–437.

74. Park, K.; Hakeem, D.A.; Cha, J.S. Synthesis and structural properties of thermoelectric Ca3−xAgxCo4O9+δ powders. Dalton Trans. 2016, 45, 6990–6997.

75. Constantinescu, G.; Madre, M.A.; Rasekh, S.; Torres, M.A.; Diez, J.C.; Sotelo, A. Effect of Ga addition on Ca-deficient Ca3Co4O9 thermoelectric materials. Ceram. Int. 2014, 40, 6255–6260.

76. Saini, S.; Yaddanapudi, H.S.; Tian, K.; Yin, Y.; Magginetti, D.; Tiwari, A. Terbium ion doping in Ca3Co4O9: A step towards high-performance thermoelectric materials. Sci. Rep. 2017, 7, 44621.

77. Bhaskar, A.; Huang, Y.C.; Liu, C. Improvement on the low-temperature thermoelectric characteristics of Ca3−xYbxCo4O9+δ (0 ≤ x ≤ 0.10). Ceram. Int. 2014, 40, 5937–5943.

78. Yang, W.C.; Qian, H.J.; Gan, J.Y.; Wei, W.; Wang, Z.H.; Tang, G.D. Effects of Lu and Ni substitution on thermoelectric properties of Ca3Co4O9+δ. J. Electron. Mater. 2016, 45, 4171–4176.

79. Wang, Y.; Sui, Y.; Ren, P.; Wang, L.; Wang, X.J.; Su, W.H.; Fan, H.J. Strongly correlated properties and enhanced thermoelectric response in Ca3Co4−xMxO9 (M = Fe, Mn, and Cu). Chem. Mater. 2009, 22, 1155–1163.

80. Huang, Y.A.; Zhao, B.C.; Lin, S.; Ang, R.; Song, W.H.; Sun, Y.P. Strengthening of thermoelectric performance via Ir doping in layered Ca3Co4O9 system. J. Am. Ceram. Soc. 2014, 97, 798–804.

81. Zhang, P.; Lou, Z.H.; Gong, L.Y.; Xu, J.; Chen, Q.; Reece, M.J.; Yan, H.X.; Dashevsky, Z.; Gao, F. High-entropy MTiO3 perovskite oxides with glass-like thermal conductivity for thermoelectric applications. J. Alloys Compd. 2023, 937, 168366.

82. Zhang, P.; Gong, L.Y.; Lou, Z.H.; Xu, J.; Cao, S.Y.; Zhu, J.T.; Yan, H.X.; Gao, F. Reduced lattice thermal conductivity of perovskite-type high-entropy (Ca0.25Sr0.25Ba0.25RE0.25)TiO3 ceramics by phonon engineering for thermoelectric applications. J. Alloys Compd. 2022, 898, 162858.

83. Zhang, P.; Lou, Z.H.; Hu, G.X.; Wu, Z.Z.; Xu, J.; Gong, L.Y.; Gao, F. In-situ construction of all-scale hierarchical microstructure and thermoelectric properties of (Sr0.25Ca0.25Ba0.25La0.25)TiO3/Pb@Bi composite oxide ceramics. J. Mater. 2023; in press.

84. Zhang, R.Z.; Gucci, F.; Zhu, H.Y.; Chen, K.; Reece, M.J. Data-driven design of ecofriendly thermoelectric high-entropy sulfides. Inorg. Chem. 2018, 57, 13027–13033.

85. Liu, R.H.; Chen, H.Y.; Zhao, K.P.; Qin, Y.T.; Jiang, B.B.; Zhang, T.S.; Sha, G.; Shi, X.; Uher, C.; Zhang, W.Q.; et al. Entropy as a gene-like performance indicator promoting thermoelectric materials. Adv. Mater. 2017, 29, 1702712.

86. Zhang, P.; Lou, Z.H.; Qin, M.H.; Xu, J.; Zhu, J.T.; Shi, Z.M.; Chen, Q.; Reece, M.J.; Yan, H.X.; Gao, F. High-entropy (Ca0.2Sr0.2Ba0.2La0.2Pb0.2)TiO3 perovskite ceramics with A-site short-range disorder for thermoelectric applications. J. Mater. Sci. Technol. 2022, 97, 182–189.

87. Zhang, P.; Lou, Z.H.; Gong, L.Y.; Xu, J.; Chen, Q.; Reece, M.J.; Yan, H.X.; Dashevsky, Z.; Gao, F. High-entropy MTiO3 perovskite oxides with glass-like thermal conductivity for thermoelectric applications. J. Alloys Compd. 2023, 937, 168366.

88. Zhang, P.; Gong, L.Y.; Lou, Z.H.; Xu, J.; Cao, S.Y.; Zhu, J.T.; Yan, H.X.; Gao, F. Reduced lattice thermal conductivity of perovskite-type high-entropy (Ca0.25Sr0.25Ba0.25RE0.25)TiO3 ceramics by phonon engineering for thermoelectric applications. J. Alloys Compd. 2022, 898, 162858.

89. Langenberg, E.; Ferreiro-Vila, E.; Leborán, V.; Fumega, A.O.; Pardo, V.; Rivadulla, F. Analysis of the temperature dependence of the thermal conductivity of insulating single crystal oxides. APL Mater. 2016, 4, 104815.

90. Yu, J.C.; Chen, K.; Azough, F.; Alvarez-Ruiz, D.T.; Reece, M.J.; Freer, R. Enhancing the thermoelectric performance of Calcium Cobaltite ceramics by tuning composition and processing. ACS Appl. Mater. Interfaces 2020, 12, 47634–47646.

91. Li, Z.; Xiao, C.; Fan, S.J.; Deng, Y.; Zhang, W.S.; Ye, B.J.; Xie, Y. Dual vacancies: An effective strategy realizing synergistic optimization of thermoelectric property in BiCuSeO. J. Am. Chem. Soc. 2015, 137, 6587–6593.

92. Sanmathi, C.S.; Takahashi, Y.; Sawaki, D.; Klein, Y.; Retoux, R.; Terasaki, I.; Noudem, J.G. Microstructure control on thermoelectric properties of Ca0.96Sm0.04MnO3 synthesised by co-precipitation technique. Mater. Res. Bull. 2010, 45, 558.

93. Lou, Z.H.; Zhang, P.; Gong, L.Y.; Xu, J.; Gong, L.Y.; Reece, M.J.; Yan, H.X.; Gao, F. A novel high-entropy perovskite ceramics Sr0.9La0.1(Zr0.25Sn0.25Ti0.25Hf0.25)O3 with low thermal conductivity and high Seebeck coefficient. J. Eur.

Ceram. Soc. 2022, 42, 3480–3488.

94. Zhang, P.; Lou, Z.H.; Gong, L.Y.; Xu, J.; Chen, Q.; Reece, M.J.; Yan, H.X.; Dashevsky, Z.; Gao, F. High-entropy MTiO3 perovskite oxides with glass-like thermal conductivity for thermoelectric applications. J. Alloys Compd. 2023, 937, 168366.
95. Devi, N.Y.; Vijayakumar, K.; Rajasekaran, P.; Nedunchezhian, A.S.A.; Sidharth, D.; Masaru, S.; Arivanandhan, M.; Jayavel, R. Effect of Gd and Nb co-substitution on enhancing the thermoelectric power factor of nanostructured SrTiO3. Ceram. Int. 2021, 47, 3201–3208.
96. Buscaglia, M.T.; Maglia, F.; Anselmi-Tamburini, U.; Marré, D.; Pallecchi, I.; Ianculescu, A.; Canu, G.; Viviani, M.; Fabrizio, M.; Buscaglia, V. Effect of nanostructure on the thermal conductivity of La-doped SrTiO3 ceramics. J. Eur. Ceram. Soc. 2014, 34, 307–316.
97. Wang, Y.F.; Fujinami, K.; Zhang, R.Z.; Wan, C.L.; Wang, N.; Ba, Y.S.; Koumoto, K. Interfacial thermal resistance and thermal conductivity in nanograined SrTiO3. Appl. Phys. Express 2010, 3, 031101.
98. Ohta, S.; Nomura, T.; Ohta, H.; Koumoto, K. High-temperature carrier transport and thermoelectric properties of heavily La- or Nb-doped SrTiO3 single crystals. J. Appl. Phys. 2005, 97, 034106.
99. Dehkordi, A.M.; Bhattacharya, S.; Darroudi, T.; Graff, J.W.; Schwingenschlogl, U.; Alshareef, H.N.; Tritt, T.M. Large thermoelectric power factor in Pr-Doped SrTiO3-δ ceramics via grain-boundary-induced mobility enhancement. Chem. Mater. 2014, 26, 2478–2485.
100. Dehkordi, A.M.; Bhattacharya, S.; He, J.; Alshareef, H.N.; Tritt, T.M. Significant enhancement in thermoelectric properties of polycrystalline Pr-doped SrTiO3−δ ceramics originating from nonuniform distribution of Pr dopants. Appl. Phys. Lett. 2014, 104, 193902.
101. Srivastava, D.; Norman, C.; Azough, F.; Schäfer, M.C.; Guilmeau, E.; Freer, R. Improving the thermoelectric properties of SrTiO3-based ceramics with metallic inclusions. J. Alloys Compd. 2018, 731, 723–730.
102. Zhang, P.; Qin, M.J.; Lou, Z.H.; Cao, S.Y.; Gong, L.Y.; Xu, J.; Reece, M.J.; Yan, H.X.; Dashevsky, Z.; Gao, F. Grain orientation evolution and multi-scale interfaces enhanced thermoelectric properties of textured Sr0.9La0.1TiO3 based ceramics. J. Eur. Ceram. Soc. 2022, 42, 7017–7026.
103. Shi, Z.M.; Su, T.C.; Zhang, P.; Lou, Z.H.; Qin, M.J.; Gao, T.; Xu, J.; Zhu, J.H.; Gao, F. Enhanced thermoelectric performance of Ca3Co4O9 ceramics through grain orientation and interface modulation. J. Mater. Chem. A 2020, 8, 19561–19572.
104. Zhang, P.; Qin, M.J.; Lou, Z.H.; Cao, S.Y.; Gong, L.Y.; Xu, J.; Reece, M.J.; Yan, H.X.; Dashevsky, Z.; Gao, F. Grain orientation evolution and multi-scale interfaces enhanced thermoelectric properties of textured Sr0.9La0.1TiO3 based ceramics. J. Eur. Ceram. Soc. 2022, 42, 7017–7026.
105. Jana, S.S.; Maiti, T. Enhanced thermoelectric performance in oxide composites of La and Nb codoped SrTiO3 by using graphite as the electron mobility booster. ACS Appl. Mater. Interfaces 2022, 14, 14174–14181.
106. Bolotin, K.I.; Sikes, K.J.; Jiang, Z.; Klima, M.; Fudenberg, G.; Hone, J.; Kim, P.; Stormer, H.L. Ultrahigh electron mobility in suspended graphene. Solid State Commun. 2008, 146, 351–355.
107. Ekren, D.; Cao, J.Y.; Azough, F.; Kepaptsoglou, D.; Ramasse, Q.; Kinloch, I.A.; Freer, R. Controlling the thermoelectric behavior of La-doped SrTiO3 through processing and addition of graphene oxide. ACS Appl. Mater. Interfaces 2022, 14, 53711–53723.
108. Dey, P.; Jana, S.S.; Anjum, F.; Bhattacharya, T.; Maiti, T. Effect of semiconductor to metal transition on thermoelectric performance in oxide nanocomposites of SrTi0.85Nb0.15O3 with graphene oxide. Appl. Mater. Today 2020, 21, 100869.
109. Yin, Y.N.; Tudu, B.; Tiwari, A. Recent advances in oxide thermoelectric materials and modules. Vacuum 2017, 146, 356–374.
110. Lim, C.H.; Choi, S.M.; Seo, W.S.; Lee, M.H.; Lee, K.H.; Park, H.H. A study of electrodes for thermoelectric oxides. Electron. Mater. Lett. 2013, 9, 445–449.
111. Tougas, I.M.; Amani, M.; Gregory, O.J. Metallic and ceramic thin film thermocouples for gas turbine engines. Sensors 2013, 13, 15324–15347.
112. Yakaboylu, G.A.; Pillai, R.C.; Sabolsky, K.; Sabolsky, E.M. Fabrication and thermoelectric characterization of transition metal silicide-based composite thermocouples. Sensors 2018, 18, 3759.
113. Repaka, D.V.M.; Suwardi, A.; Kumar, P. New paradigm for efficient thermoelectrics. In Energy Saving Coating Materials; Elsevier: Amsterdam, The Netherlands, 2020; pp. 183–196.

114. Kraemer, D.; Poudel, B.; Feng, H.P.; Caylor, J.C.; Yu, B.; Yan, X.; Ma, Y.; Wang, X.W.; Wang, D.Z.; Muto, A.; et al. High-performance flat-panel solar thermoelectric generators with high thermal concentration. Nat. Mater. 2011, 10, 532–538.